Supporting Information for:

Seasonal Analysis of Reduced and Oxidized Nitrogen-Containing Organic Compounds at a Coastal Site

Jenna C. Ditto[1,†], Jo Machesky[1], and Drew R. Gentner[1,*]

[1] Department of Chemical and Environmental Engineering, Yale University,
New Haven, CT, 06511, USA

[†] Now at: Department of Chemical Engineering and Applied Chemistry, University of Toronto,
Toronto, ON, M5S 3E5, Canada

* Correspondence to: drew.gentner@yale.edu

S1. Sampling and Analytical Methods for Functionalized Gases Using PEEK Collectors and LC-ESI-MS

S1.1. Background

Many functionalized gas-phase organic compounds are challenging to measure with GC methods. This is because their higher polarity, chemical functionality, stability, and/or thermal lability can lead to difficulties with thermal desorption from sampling media, irreversible losses in the GC column's active phase and other system components, or unintended analyte transformations. Some studies using GC for the separation of functionalized compounds employ derivatization prior to analysis to improve separation and detection. However, derivatization is known to cause undesired side reactions and can only be used to alter a select subset of functional groups that respond predictably when mixed with derivatizing agents. Alternative methods for the analysis of higher polarity gas-phase compounds collected on sampling substrates have been used in past work, which often involve solvent extraction instead of thermal desorption, and subsequent analysis via GC- or LC-MS (Chu et al., 2016; Harper, 2000; Ramírez et al., 2010; Ras et al., 2009). This can be more effective when compounds are thermally labile, though extraction into solution can be time consuming, and selecting a safe but effective solvent for extraction of a broad range of analytes presents an additional challenge.

Here, samples collected on pre-cleaned, cooled PEEK tubing were desorbed directly into the LC flow path using the LC mobile phase (without any additional sample preparation methods), then trapped/focused on the LC column, separated, and finally analyzed with ESI-MS. Inline LC mobile phase desorption with ESI-MS analysis provides a gentle and efficient mechanism for the desorption and separation/analysis of polar analytes that are typically not GC amenable. This method also avoids a separate extraction (and thus dilution step), allowing for the detection of lower concentration analytes.

S1.2. Sampling on Cooled PEEK Collectors

We used PEEK tubing as an adsorptive sampler for functionalized gas-phase compounds. To cool the adsorptive sampler, we inserted the PEEK tubing (1/16” OD, 0.04” ID, 2.75” long, resulting in a volume of 0.06 mL) into a piece of aluminum tubing (1/8” OD, 1/16” ID) to jacket the PEEK collector, and placed the ensemble into an aluminum block (2” x 1.25”) through a 1/8” hole cut through the center of the block. The PEEK tubing outer diameter and length were selected to match the dimensions of the aluminum cooling block while maintaining a straight flow path. The block was insulated and cooled to 2°C with a Peltier cooler (Custom Thermoelectric, 1.5” x 1.5”). We selected 2°C to maximize trapping efficiency (due to a decrease in analyte vapor pressure, discussed below), to maintain a thin liquid layer of water in the tubing, but to avoiding freezing water and potentially clogging the line. We also tested lower temperatures (e.g. -15°C) in follow-up laboratory experiments to inform future developments of this method. Temperature was monitored by a thermocouple in the aluminum block and controlled by a proportional-integral-derivative (PID) controller (Omega CN742). A pump was connected downstream of the PEEK tubing and flow controller. We set flow through the PEEK tubing with an Alicat mass flow controller, and limited air flow to 22 mL/min to maintain laminar flow and provide sufficient time for gas diffusion to the inner tubing walls.

S1.3. Inline LC Mobile Phase Desorption and LC-ESI-MS Analysis

After sampling in the field (or in the laboratory), PEEK collectors were installed directly inline with the LC column for analyte desorption and analysis. We used a multi-position valve to pass flow through or to circumvent the PEEK tubing (Figure 1 in the main manuscript). To desorb analytes, we held the mobile phase composition at 95% water and 5% methanol at 0.05 mL/min for 20 minutes, similar to methods employed in other fields that use LC column loading steps to study other forms of complex mixtures (Alvarez-Segura et al., 2016; Greco et al., 2013; Pyke et al., 2015). In this step, analytes were desorbed from the PEEK tubing and subsequently trapped and focused on the LC column (Figure 1Ai, Table S1 line 1); compounds with good affinity to the C18 column stationary phase were successfully trapped and focused (e.g. low- to moderate-polarity functionalized species with larger molecular weight), while very water soluble species were not focused well (Table S2). We used a 20 minute hold time to maximize desorption from the PEEK collector tubing (by allowing the solvent in the PEEK tubing to be exchanged ~20 times), while minimizing early elution from the LC column during this trapping step. This leveraged the very low flow rate through the column and the high water content of the mobile phase, whose eluent strength was not sufficient to allow much elution from the reverse phase LC column. In cases of early elution (i.e. elution from the column during the 20 minute hold period with very low flow rate through the column), peak shape was very poor, and thus peak identification in later analysis was challenging. Thus, when longer hold periods were tested and showed more early elution from the LC column, they were not pursued further either. We also note that we evaluated a shorter hold period of 5 minutes during testing, but this did not show sufficient desorption from the PEEK tubing.

At 20 minutes, the multi-position valve was switched to position "b" (Figure 1Aii), to circumvent the PEEK tubing. At this point, the flow rate was increased to 0.3 mL/min and went straight to the LC column, desorbing compounds from the column stationary phase and carrying them to the mass spectrometer following the gradient in Table S1.

An Agilent Poroshell 120 EC-C18 column (3.0 x 50 mm, 2.7 Micron) with a C18 guard column (3.0 x 5 mm, 2.7 Micron) were used for analyte focusing and chromatography, in an Agilent 1260 Infinity HPLC system. We note that this is a different column than the SB-Aq column used for particle-phase measurements, though a comparison of analyte retention times showed similar behavior across columns.

Ionization was performed with an electrospray source (ESI), and samples were analyzed with an Agilent 6550 Q-TOF in positive ionization mode. Methanol (≥99.9% purity, Sigma-Aldrich) and water (Milli-Q, 18.2 MΩ·cm, <3 ppb TOC) were used as LC mobile phases, with 0.1% acetic acid (for HPLC, Sigma-Aldrich) as a modifier. ESI and Q-TOF parameters are discussed in detail in past work (Ditto et al., 2018). In brief, the ESI source drying gas was operated at 225°C and 17 L/min, with a fragmentor and capillary voltage of 365 V and 4000 V respectively, and a sheath gas flow of 12 L/min at 400°C. The Q-TOF scanned for ions between *m/z* 50-1000, at 4 spectra/second. A solution of reference masses from Agilent Technologies (5 mM purine and 2.5 mM HP-0921 in 95% acetonitrile (≥99.9% purity, Honeywell) and 5% water

(Milli-Q, 18.2 MΩ·cm, <3 ppb TOC)), was introduced to the Q-TOF throughout the entire LC elution time to reduce ion mass drift.

S1.4. Method Evaluation

To evaluate desorption from the PEEK tubing over the 20 minute desorption time and the effectiveness of trapping/focusing on the LC column, we spiked pieces of PEEK tubing with a range of liquid standards (e.g. 10 ng/μL each of several functionalized species such as carboxylic acids, phthalates, alcohols, and a range of nitrogen- or sulfur-containing compounds, selected to cover a range of atmospherically-relevant functional groups and compound sizes that could be observed in the gas- or particle-phase, see Table S2). This spiked PEEK tubing was then desorbed immediately in the inline desorption system.

A comparison of peak areas from spiked PEEK experiments to peak areas from a typical LC run with standard injection (i.e. without PEEK tubing in the flow path) for the same standard suggests that most compounds were effectively desorbed from the PEEK during the 20 minute inline desorption period (71% ± 23% recovery). Also, most compounds from the spiked PEEK experiment showed a 20 minute delay from their expected retention time observed during a typical LC run (Figure 1B and Table S2). We discuss these recovery results more below.

To evaluate compound breakthrough, we cooled pieces of PEEK tubing to 2°C in the Peltier cooler setup discussed above, and challenged them with a series of breakthrough volumes. The standard shown in Table S2 was spiked into the inlet of the cooled PEEK tubing with a glass syringe. Liquid standards were used here instead of gaseous standards since these functionalized standards were not available to mix in a compressed gas cylinder, and volatilization was avoided to limit thermal degradation or other reactive losses during evaporation. Air flow at 22 mL/min was maintained through the 2°C block for 30 minutes, 1 hour, 2 hours, 2.5 hours, and 3 hours, and each sample was analyzed on the LC-ESI-MS system with inline analyte desorption from the PEEK tubing. Analyte breakthrough became significant at 2.5-3 hours. After 2 hours of air flow (equivalent to 2.64 L), breakthrough was limited to 20% or less (i.e. breakthrough test peak areas were 80% ± 27% on average compared to those from a typical LC run without PEEK tubing in line, though a range of behaviors was observed, see Table S2). Thus, 2 hours was set as the maximum sampling time for this method.

There are several factors that could potentially influence weaker analyte retention or recovery from the PEEK samplers. For example, compounds with higher volatility could evaporate from the PEEK collector prior to LC analysis; this possible behavior is seen in cases where signal was lower for the spiked PEEK test compared to the cooled breakthrough test (e.g. pyrogallol, Table S2). In these cases, higher volatility species likely evaporated from the spiked PEEK, as they were not distributed across the cooled PEEK tubing and thus likely did not adsorb as effectively as they may have during the breakthrough test. Matrix effects with other analytes in the test mixture could have also contributed to these differences.

Conversely, compounds with minimal functionality may have adsorbed less effectively to the cooled PEEK surface during breakthrough testing (e.g. benzophenone, Table S2), some compounds may have been irreversibly taken up by the PEEK surface in the absence of solvent, and some compounds may have suffered from chemical incompatibility with PEEK (though PEEK is generally considered to be quite inert and often is used in standard LC system flow paths). These factors may have contributed to compounds with lower breakthrough testing signals, but good recovery from the spiked PEEK experiment without breakthrough testing.

Also, after mobile phase desorption from the PEEK tubing, some analytes were poorly retained in the LC column and eluted during the trapping/focusing stage (e.g. pyrogallol, xylitol, mannose). These compounds thus had poor peak shape, since they eluted with very low flow rate through the LC column (0.05 mL/min), and their peaks were therefore challenging to integrate. As such, data from these early-eluting compounds may still be used qualitatively, though a quantitative assessment of their abundances is difficult, and future work may employ other more specialized columns for polar analytes to resolve this.

We did not observe many functionalized compounds in the VOC volatility range in our ambient samples, but we expect challenges with trapping high volatility species in the cooled PEEK tubing at 2°C. In past studies investigating the delay time exhibited in various types of tubing by compound volatility, the volatility of individual compounds was inversely related to their delay time in PEEK tubing: higher volatility species exhibited shorter delays (Deming et al., 2019; Pagonis et al., 2017). Past characterization of PEEK suggests that lightly functionalized VOCs (they studied ketones with $C_0 > 10^6$ $\mu g/m^3$ (Donahue et al., 2011)) are delayed by ~60 seconds/meter of tubing at room temperature (~295 K) (Deming et al., 2019), which would translate to a delay of just ~4 seconds in the 7 cm (2.75”) of PEEK used here if the PEEK were held at room temperature. While this delay time would be lengthened if the PEEK were held at lower temperature, e.g. the 2°C setpoint that we used in this study, this delay time is still short and thus indicates that VOCs would likely not be effectively trapped in PEEK tubing used as a sampler unless cooled to much lower temperatures. For comparison, by extrapolating from Deming et al.’s analysis of PEEK tubing at room temperature, which showed data for some IVOCs but mostly focused on VOCs, we note that less volatile IVOCs ($C_0 \sim 300$ $\mu g/m^3$) and SVOCs ($0.3 < C_0 < 300$ $\mu g/m^3$) (Donahue et al., 2011) may remain adsorbed to tubing walls for 1+ hours/meter, and likely longer if cooled due to decreasing volatility with temperature (in combination with possible changes in the adsorptive properties of PEEK, uptake to condensed water, and the more minor effect of changes in gas-phase diffusivity with temperature (Pagonis et al., 2017)).

Here, we demonstrate this method as a qualitative approach to probe understudied functionalized gases in the atmosphere and use it to examine the presence of functionalized gas-phase organic compounds, but acknowledge that for highly quantitative measurements, future work is required to further optimize this sampling and analysis system for compounds of interest. Future developments of this PEEK collector setup could allow for larger sampling volumes, and thus lower limits of detection, by coiling tubing to increase trapping length. Other opportunities include evaluating lower temperatures for trapping, increasing the surface area used for adsorption, and exploring different types of adsorptive surfaces with different functionality. Different LC columns for trapping and analysis could be used; larger volume columns could be employed if longer periods were needed for PEEK desorption, and different column composition and mobile phases could be explored to trap and focus analytes with different molecular properties. This method could also be fine-tuned to sample and analyze select compound classes of interest, for example, per- and polyfluoroalkyl substances (PFAS). As an avenue of exploratory method development, we evaluated the system with a challenge mixture of PFAS species to test the system's ability to sample and analyze these highly fluorinated compounds (Table S3). We note that ambient PFAS measurements were outside of the scope of this study, but describe this as an example of other extended applications of this sampling and analytical methodology.

S2. Further YCFS Site Characterization

The Long Island Sound region is often in non-attainment for O_3 in the summer months due to a mix of pollutant transport up the coast from large East Coast metropolitan areas, regional biogenic emissions, and summertime chemical processing. In the summer of 2018 during sampling, there were several high O_3 events observed. In the summer, O_3 mixing ratios showed a strong diurnal variation, with maximum mixing ratios (computed over corresponding 8 hour filter sampling periods) reaching 57 ± 20 ppb on average. In contrast, wintertime O_3 during the sampling period was more consistent and did not exhibit the same characteristic diurnal patterns driven by photochemistry. Winter maxima were 46 ± 5 ppb and showed some decreases during periods of higher NO_x concentrations due to O_3 titration. Biogenic VOC emissions and actinic fluxes were reduced in the winter, which are both crucial to O_3 formation and which have been also shown to extend wintertime NO_x lifetimes in the Northeast U.S. (Kenagy et al., 2018).

This decrease in biogenic VOC contributions was observed in the gas-phase adsorbent tube data, where gas-phase CH species (i.e. fully reduced hydrocarbons) played a more important role in summer (24% of detected ion abundance) than in winter (18%). This difference could also be related to larger contributions of fresh emissions from urban cores during the summer. The greater prevalence of fresh emissions in summer led to summertime samples showing typically lower average molecular weight (summer: 156 ± 58 g/mol, vs. winter 200 ± 74 g/mol, $p < 0.05$) and predictably higher saturation mass concentrations (summer: $\log(C_0) = 5.3 \pm 2.1\ \mu g/m^3$, vs. winter: $\log(C_0) = 3.8 \pm 2.6\ \mu g/m^3$, $p < 0.05$) than wintertime samples. However, with more fresh VOC emissions in summer combined with increased photochemistry, gas-phase oxygen-to-carbon ratios (O/C) were slightly higher in the summer relative to winter (summer: 0.2 ± 0.2, vs.

winter: 0.1 ± 0.1, $p < 0.05$), driven up by a larger contribution from C_3-C_6 compounds with higher O/C in summer. These C_3-C_6 compounds are discussed more in the main text.

Together, this decrease in biogenic VOC precursor concentration, reduced sunlight, and greater persistence of NO_x likely all contributed to the more consistent wintertime O_3 concentrations observed, in contrast with the clear diurnal trends observed in the summer.

Backward trajectories on days where summertime O_3 measurements exceeded National Ambient Air Quality Standards tended to be from the southwest or west, highlighting well-known influence from East Coast metropolitan areas on coastal Connecticut and other downwind regions. However, backward trajectories from the northwest were also present on some of these non-attainment days, emphasizing the role of other regional urban emissions, mixing, and local chemistry in the region.

Summertime concentrations for $PM_{2.5}$ and BC were higher than winter (i.e. 10.0 vs. 7.4 $\mu g/m^3$ for $PM_{2.5}$, respectively; 0.5 vs 0.2 $\mu g/m^3$ for BC, respectively), indicating the possibility of additional emissions or transport (e.g. due to long-distance transport of biomass burning emissions observed at the site (Rogers et al., 2020)) and increased secondary formation of $PM_{2.5}$ with increased chemical processing in summer.

S2.1. Further Notes on Aerosol Liquid Water Estimates

We used O/C to estimate the hygroscopicity parameter, κ, which averaged to 0.17 ± 0.06 in summer vs. 0.11 ± 0.03 in winter ($p < 0.05$), and fell within the expected range of 0.01-0.5 in the literature (DeRieux et al., 2018; Petters and Kreidenweis, 2007). Using the IMPROVE Network's $PM_{2.5}$ speciation data from the Mohawk Mountain site in Connecticut in summer (July-August 2018) and winter (February-March 2019), we estimated organic-derived aerosol liquid water using the hygroscopicity parameter approach (Petters and Kreidenweis, 2007), and found a higher organic-derived aerosol liquid water content in summer, consistent with increased hygroscopicty in summer. Estimated organic-derived aerosol liquid water concentrations were on average 0.8 μg/m^3 in summer vs. 0.2 μg/m^3 in winter ($p < 0.05$).

With ammonium sulfate, ammonium nitrate, and sea salt concentrations from IMPROVE data (assuming sea salt was dominated by sodium chloride), we used ISORROPIA to estimate the contribution of inorganic-liquid water similar to past work (Slade et al., 2019). We found no statistically significant difference between summer and winter inorganic-derived aerosol liquid water (on average 1.6 μg/m^3 in summer vs. 1.5 μg/m^3 in winter, $p > 0.05$). Overall, total estimated aerosol liquid water was higher in summer than in winter in the region (on average 2.4 μg/m^3 in summer vs. 1.7 μg/m^3 in winter, $p < 0.05$). While we observed more noticeable indicators of aqueous-phase processing in winter despite lower calculated aerosol liquid water, this is perhaps because there were fewer competing photochemical processes in winter, as discussed in the main text.

S3. Additional Functional Group Speciation for Other N-Containing Compound Classes

S3.1. CHONS

Similar to the other nitrogen-containing compound classes, we observed significantly more CHONS at this site than at past studied ambient sites (i.e. 20% of detected functionalized organic aerosol ion abundance in summer vs. 21% in winter, Figure 3A-B). CHONS compounds in summer and winter both showed a sizable contribution from sulfonamides, which contain oxygen, nitrogen, and sulfur atoms (and contributed to 24-27% of CHONS species). However, we also observed a wide range of other functional groups that contributed to this compound class containing oxygen, nitrogen, *or* sulfur, suggesting that once again, this compound class was composed of a combination of different functional groups and structural features (Figure S4). This is consistent with our past observations of CHONS species, which showed an important contribution from sulfide groups in combination with other heteroatom-containing moieties (Ditto et al., 2021).

S3.2. CHNS

While this compound class contributed minorly overall at this site (i.e. 1% in summer, vs. 2% in winter, Figure 3A-B), it comprised a range of nitrogen- and sulfur-containing functional groups in various combinations shown in Figure S4 including amines (summer: 50% vs. winter: 68% of CHNS species), and an important contribution from nitrogen- and sulfur-containing azoles in summer (summer: 32% vs. winter: 2% of CHNS species). Imidazole (a nitrogen-containing azole) is known to form from carbonyls and nitrogen-containing compounds like ammonia or amines in the aqueous phase (DeHaan et al., 2009), as discussed in the main text. This suggests that perhaps similar pathways with sulfur-containing precursors could be involved in the formation of the nitrogen- and sulfur-containing azoles observed here.

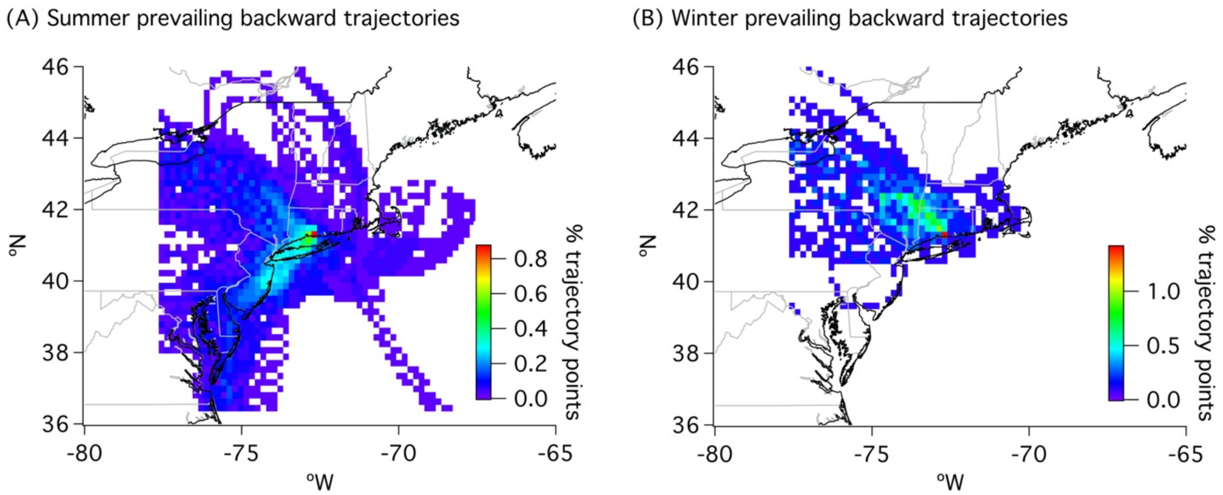

Figure S1. (A) HYSPLIT backward trajectories for summertime samples showed prevailing backward trajectories from the southwest, west, and northwest. (B) Backward trajectories in wintertime samples were predominantly from the northwest. For (A-B), HYSPLIT backward trajectories were computed and the number of trajectories passing through each defined 20 km x 20 km bin was tallied and depicted as the color scale. These results are similar those from a 2016 study at Brookhaven National Laboratory (Zhou et al., 2016), which also showed a broad distribution of trajectory directions in their summertime measurements.

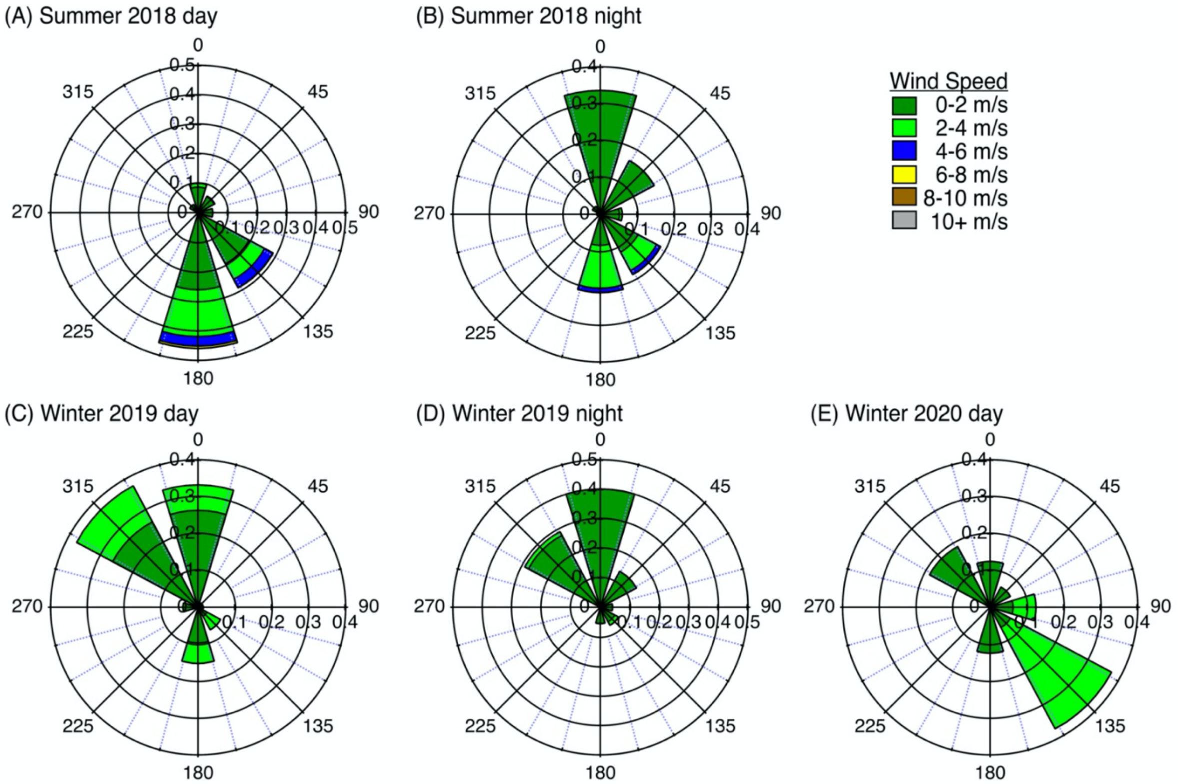

Figure S2. (A-B) Local wind roses for the summer sampling period in 2018, (C-D) for the winter sampling period in 2019, and (E) for the winter sampling period for gas-phase LC-ESI-MS measurements in 2020, where S and SE represent flow coming immediately off of the water.

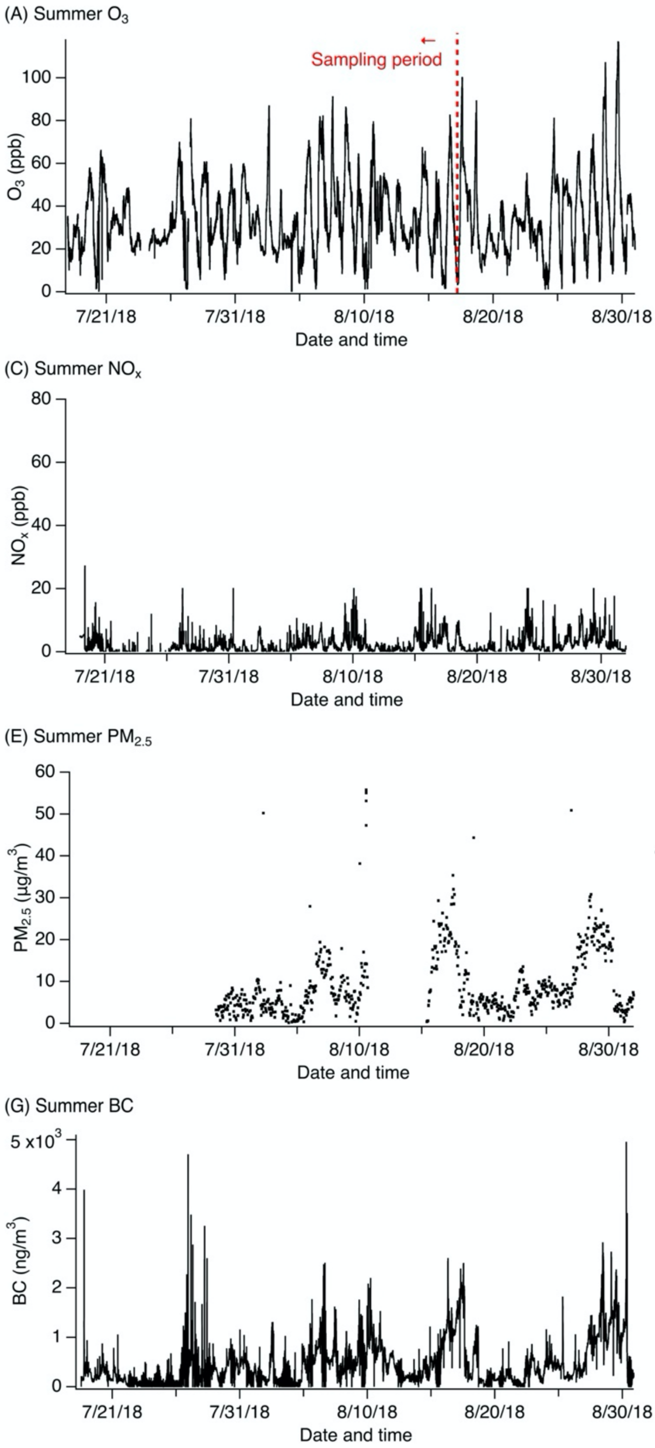

Figure S3. Time series for (A-B) O_3, (C-D) NO_x, (E-F) $PM_{2.5}$, and (G-H) black carbon (BC) concentrations. O_3 and NO_x data are shown as 1-minute averages, $PM_{2.5}$ data are reported hourly, and BC data are shown as 5 minute averages. Sampling was performed in the summer (7/9/2018-8/29/2018) and winter (2/25/2019-3/5/2019), but extended summertime dates are shown here (to the right of the red dotted line in (A)) to provide further context for pollutant concentrations at the site.

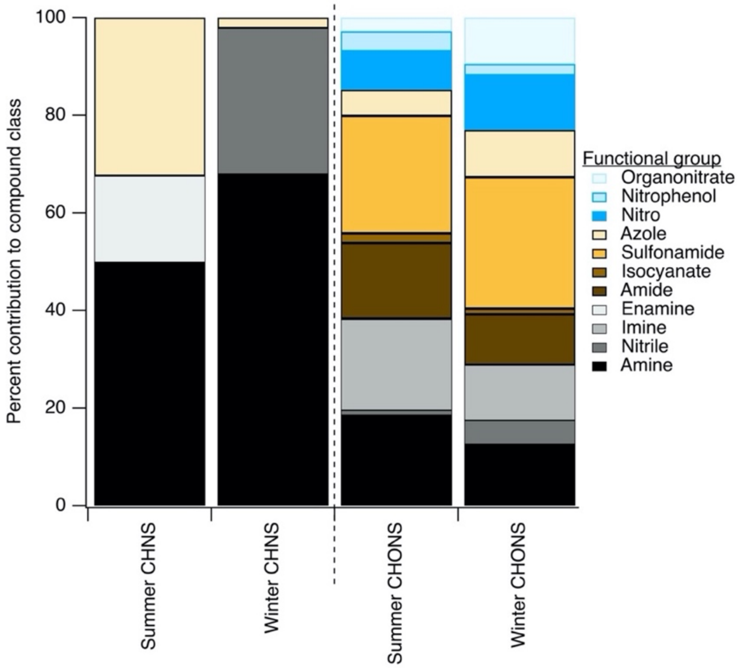

Figure S4. Functional group distribution for additional nitrogen-containing compound classes to accompany Figure 4.

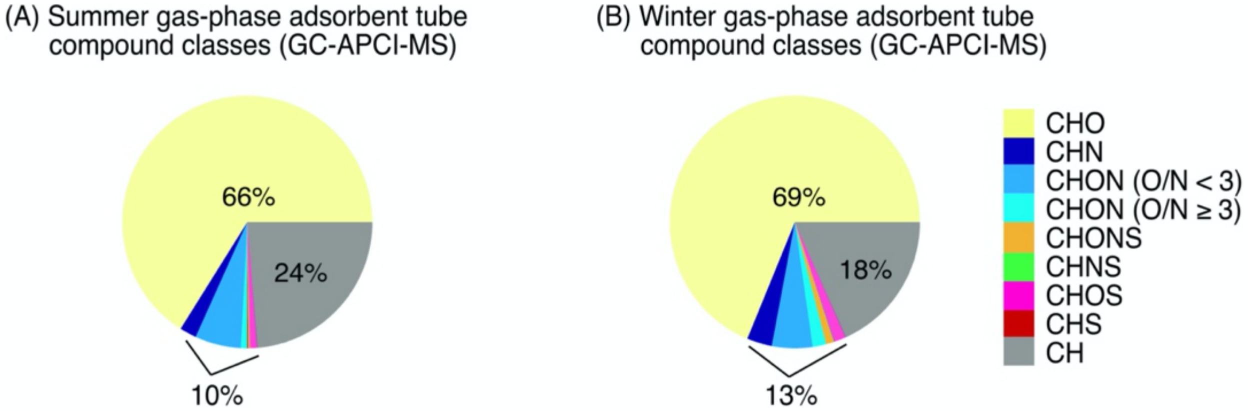

Figure S5. Adsorbent tube compound class distribution from GC-APCI-MS analysis. Non-targeted GC-APCI-MS results of (A) summer (N=34) and (B) winter (N=14) samples were dominated by CH and CHO compound classes, with only 9% of detected ion abundance in summer and 11% in winter containing a nitrogen atom. We note that given the relative susceptibility of alkanes to fragmentation in the APCI source (Khare et al., 2019), along with the configuration of the adsorbent tubes and GC, which were not optimized for light hydrocarbons (Sheu et al., 2018), the contributions of CH species here were a lower limit estimate and thus not our focus here.

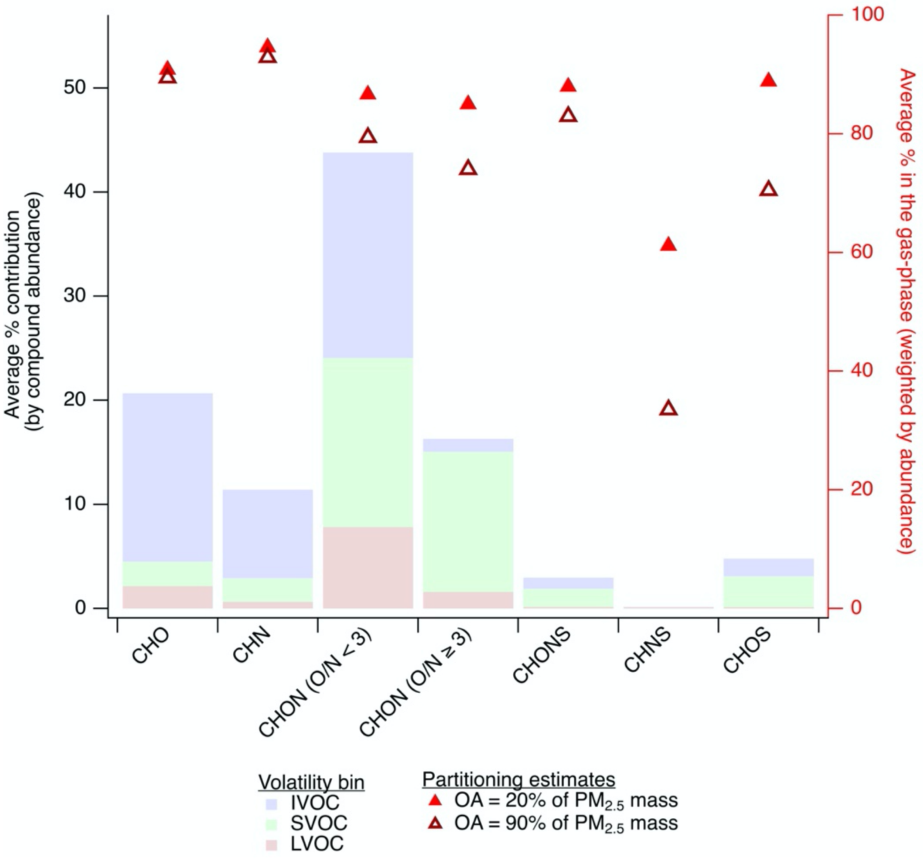

Figure S6. Predicted partitioning of compounds observed in gas-phase LC-ESI-MS data. Stacked bars and left axis are the same as in Figure 5A. Red triangle markers corresponding to the right axis were added here, to predicted phase partitioning of the functionalized gases observed from PEEK tubing samples. For these calculations, we used partitioning theory (Donahue et al., 2009) and average $PM_{2.5}$ concentration during the sampling period. We assumed that these compounds partitioned to the particle phase via condensation onto pre-existing organic aerosol, and did not include dissolution into aerosol liquid water or cloud/fog water due to uncertainty in ambient water concentrations at the site at the time of sampling. This therefore likely represents a lower bound estimate of the expected distribution across phases, since the exact role of water in influencing partitioning at this site is uncertain. We considered two extreme scenarios, where organic aerosol comprised 20% of $PM_{2.5}$ and 90% of $PM_{2.5}$ concentrations, similar to past established ranges (Jimenez et al., 2009).

Table S1. Mobile phase gradient and flow used to study functionalized gases with the inline desorption and LC-ESI-MS setup.

Time	**%A (water)**	**%B (methanol)**	**Flow rate (mL/min)**	**Method stage**
0-20 min	95	5	0.05	PEEK desorption, analyte trapping/focusing on LC column
20-20.5 min	95	5	0.05 → 0.3	Flow rate adjustment
20.5-22.5 min	95	5	0.3	LC separation
22.5-42.5 min	95 → 10	5 → 90	0.3	LC separation
42.5-47.5 min	10	90	0.3	LC separation
47.5-48.5 min	10 → 95	90 → 5	0.3	Preparation for next run
48.5-53.5 min	95	5	0.3	Column re-equilibration

Table S2. Method evaluation for PEEK collectors held at 2°C, challenged with functionalized authentic standards. Compounds denoted by * showed poor retention in the LC column, eluting during the trapping/focusing stage. Positive and negative mode typical LC runs (i.e. with no PEEK collector in flow path), spiked PEEK experiments, and breakthrough tests were performed in triplicate. Standard deviations show propagated uncertainty from the replicate typical LC runs and the spiked PEEK or breakthrough test runs. Results are shown as a percentage ± standard deviation retained relative to the typical LC runs (i.e. "LC run" below).

Compound name	Formula	Molecular weight (g/mol)	Retention time with inline PEEK desorption (min)	Ionization mode	Spiked PEEK area/LC run area (%)	2 hour break-through test area/LC run area (%), 2°C
Xylitol*	$C_5H_{12}O_5$	152.2	6.4	+	26±18%	18±18%
1,2-Dihydroxybenzene	$C_6H_6O_2$	110.1	31.2	+	116±12%	100±12%
Pyrogallol*	$C_6H_6O_3$	126.1	30.0	-	41±30%	92±2%
Levoglucosan	$C_6H_{10}O_5$	162.1	7.3	+	84±2%	95±21%
Mannose*	$C_6H_{12}O_6$	180.2	6.5	+	74±10%	73±10%
4-Methoxyphenol	$C_7H_8O_2$	124.1	38.6	+	84±17%	91±25%
Vanillin	$C_8H_8O_3$	152.2	30.8	+	77±33%	59±15%
2,6-Dimethoxyphenol	$C_8H_{10}O_3$	154.2	31.0	+	75±8%	68±25%
Vanillic Acid	$C_8H_8O_4$	168.1	29.9	-	92±19%	90±4%
Dimethylbenzylamine	$C_9H_{13}N$	135.2	15.6	+	96±29%	75±24%
Nopinone	$C_9H_{14}O$	138.2	34.5	+	84±22%	132±19%
Acetovanillone	$C_9H_{10}O_3$	166.2	32.0	-	60±13%	38±24%
Syringic Acid	$C_9H_{10}O_5$	198.2	31.0	-	83±22%	99±4%
Limonene Epoxide	$C_{10}H_{16}O$	152.2	36.9	+	72±19%	98±23%
Pinonic Acid	$C_{10}H_{16}O_3$	184.2	40.0	-	80±16%	49±2%
Dimethyl Phthalate	$C_{10}H_{10}O_4$	194.2	38.1	+	51±27%	84±25%
Camphor Sulfonic Acid	$C_{10}H_{16}SO_4$	232.3	30.8	+	100±13%	112±32%
Dodecanenitrile	$C_{12}H_{23}N$	181.3	31.4	+	18±40%	87±1%
N,N-Diethyl-Meta-Toluamide	$C_{12}H_{17}NO$	191.3	37.6	+	77±22%	79±19%
Diethyl Phthalate	$C_{12}H_{14}O_4$	222.2	38.1	+	62±23%	103±26%
Benzophenone	$C_{13}H_{10}O$	182.2	39.6	+	51±33%	21±23%
Dibutyl Phthalate	$C_{16}H_{22}O_4$	278.3	43.0	+	94±14%	102±34%
Benzyl Butyl Phthalate	$C_{19}H_{20}O_4$	312.4	43.0	+	54±26%	85±17%
Dehydroabietic Acid	$C_{20}H_{28}O_2$	300.4	45.6	-	56±4%	73±8%

Table S3. Method evaluation for PEEK collectors held at 2°C and -15°C, challenged with PFAS authentic standards. Tests at -15°C were performed specifically for PFAS standards to improve trapping in the PEEK collector, which was noticeably lower than the average trapping efficiency of the PEEK collector for the non-PFAS functionalized species. Negative mode typical LC runs (i.e. with no PEEK collector in flow path), spiked PEEK experiments, and breakthrough tests were performed in triplicate. Standard deviations show propagated uncertainty from the replicate typical LC run and the spiked PEEK or breakthrough test runs. Results are shown as a percentage ± standard deviation retained relative to the typical LC run (i.e. "LC run" below). Testing was also performed to ensure no carryover of PFAS standards between runs.

Compound name	Formula	Molecular weight (g/mol)	Retention time with inline PEEK (min)	Ion-ization mode	Spiked PEEK area/LC run area (%)	2 hour break-through test area/LC run area (%), 2°C	2 hour break-through test area/LC run area (%), -15°C
Perfluoro-n-butanoic acid	$C_4HF_7O_2$	214.0	27.6	-	104±26%	24±37%	70±18%
Perfluoro-n-pentanoic acid	$C_5HF_9O_2$	264.1	35.8	-	111±22%	20±37%	87±24%
Perfluoro-n-hexanoic acid	$C_6HF_{11}O_2$	314.1	39.2	-	89±13%	32±37%	90±9%
Perfluro-n-heptanoic acid	$C_7HF_{13}O_2$	364.1	40.5	-	85±18%	57±38%	98±10%
Perfluoro-n-octanoic acid	$C_8HF_{15}O_2$	414.1	41.9	-	97±20%	56±33%	90±16%
Perfluoro-n-nonanoic acid	$C_9HF_{17}O_2$	464.1	43.2	-	96±16%	53±27%	95±10%
Perfluoro-n-decanoic acid	$C_{10}HF_{19}O_2$	514.1	44.1	-	105±14%	64±38%	114±12%
Perfluoro-n-undecanoic acid	$C_{11}HF_{21}O_2$	564.1	45.3	-	81±26%	80±21%	88±17%
N-Methylperfluoro-octanesulfon-amidoacetic acid	$C_{11}H_6F_{17}NO_4S$	571.2	44.3	-	97±3%	19±17%	58±22%
Perfluoro-n-dodecanoic acid	$C_{12}HF_{23}O_2$	614.1	46.4	-	128±3	77±3%	66±13%
N-Ethylperfluoro-octanesulfon-amidoacetic acid	$C_{12}H_8F_{17}NO_4S$	585.2	44.6	-	97±10%	23±10%	21±7%

Table S4. Fraction of volatility bin contents estimated to be in the particle phase at 300 K (average summer sampling period temperature) and at 270 K (average winter sampling period temperature). Volatility bins defined at the 300 K reference temperature (i.e. bins shown in Figure 2) were shifted according to the Clausius Clapeyron equation from 300 K to 270 K, assuming an average enthalpy of vaporization of 100 kJ/mol (Donahue et al., 2006). This resulted in a decrease of approximately two orders of magnitude in saturation mass concentration at 270 K relative to 300 K. Partitioning to a pre-existing condensed phase was estimated according to Donahue et al. (Donahue et al., 2006) using average summertime and wintertime $PM_{2.5}$ measurements from the site and C* defined at 300 K for summer and 270 K for winter. Note, the volatility bins are held at a reference condition of 300 K for comparison between seasons in Figure 2, and are similarly shown as C* at 300 K here.

C* (μg/m^3 at 300 K)	Fraction in particle phase at 300 K	Fraction in particle phase at 270 K	Volatility bin at 300 K
1.00E+06	0.00	0.00	IVOC
1.00E+05	0.00	0.01	IVOC
1.00E+04	0.00	0.06	IVOC
1.00E+03	0.01	0.39	IVOC
1.00E+02	0.09	0.86	SVOC
1.00E+01	0.50	0.98	SVOC
1.00E+00	0.91	1.00	SVOC
1.00E-01	0.99	1.00	LVOC
1.00E-02	1.00	1.00	LVOC
1.00E-03	1.00	1.00	LVOC
1.00E-04	1.00	1.00	LVOC
1.00E-05	1.00	1.00	ELVOC
1.00E-06	1.00	1.00	ELVOC

References

Alvarez-Segura, T., Torres-Lapasio, J. R., Ortiz-Bolsico, C. and García-Alvarez-Coque, M. C.: Stationary phase modulation in liquid chromatography through the serial coupling of columns: A review, Anal. Chim. Acta, 923, 1–23, doi:10.1016/j.aca.2016.03.040, 2016.

Chu, L., Deng, S., Zhao, R., Deng, J. and Kang, X.: Comparison of Adsorption/Desorption of Volatile Organic Compounds (VOCs) on Electrospun Nanofibers with Tenax TA for Potential Application in Sampling, PLoS One, 11(10), 1–14, doi:10.1371/journal.pone.0163388, 2016.

DeHaan, D. O., Corrigan, A. L., Smith, K. W., Stroik, D. R., Turley, J. J., Lee, F. E., Tolbert, M. A., Jimenez, J. L., Cordova, K. E. and Ferrell, G. R.: Secondary Organic Aerosol-Forming Reactions of Glyoxal with Amino Acids, Environ. Sci. Technol., 43(8), 2818–2824, doi:10.1021/es803534f, 2009.

Deming, B. L., Pagonis, D., Liu, X., Day, D. A., Talukdar, R., Krechmer, J. E., de Gouw, J. A., Jimenez, J. L. and Ziemann, P. J.: Measurements of delays of gas-phase compounds in a wide variety of tubing materials due to gas–wall interactions, Atmos. Meas. Tech., 12(6), 3453–3461, doi:10.5194/amt-12-3453-2019, 2019.

DeRieux, W.-S. W., Li, Y., Lin, P., Laskin, J., Laskin, A., Bertram, A. K., Nizkorodov, S. A. and Shiraiwa, M.:

Predicting the glass transition temperature and viscosity of secondary organic material using molecular composition, Atmos. Chem. Phys., 18(9), 6331–6351, doi:10.5194/acp-18-6331-2018, 2018.

Ditto, J. C., Barnes, E. B., Khare, P., Takeuchi, M., Joo, T., Bui, A. A. T., Lee-Taylor, J., Eris, G., Chen, Y., Aumont, B., Jimenez, J. L., Ng, N. L., Griffin, R. J. and Gentner, D. R.: An omnipresent diversity and variability in the chemical composition of atmospheric functionalized organic aerosol, Commun. Chem., 1(1), 75, doi:10.1038/s42004-018-0074-3, 2018.

Ditto, J. C., He, M., Hass-Mitchell, T. N., Moussa, S. G., Hayden, K., Li, S.-M., Liggio, J., Leithead, A., Lee, P., Wheeler, M. J., Wentzell, J. J. B. and Gentner, D. R.: Atmospheric Evolution of Emissions from a Boreal Forest Fire: The Formation of Highly-Functionalized Oxygen-, Nitrogen-, and Sulfur-Containing Compounds, Atmos. Chem. Phys., 21, 255–267, 2021.

Donahue, N. M., Robinson, A. L., Stanier, C. O. and Pandis, S. N.: Coupled Partitioning, Dilution, and Chemical Aging of Semivolatile Organics, Environ. Sci. Technol., 40(8), 2635–2643, doi:10.1021/ES052297C, 2006.

Donahue, N. M., Robinson, A. L. and Pandis, S. N.: Atmospheric organic particulate matter: From smoke to secondary organic aerosol, Atmos. Environ., 43(1), 94–106, doi:10.1016/j.atmosenv.2008.09.055, 2009.

Donahue, N. M., Epstein, S. A., Pandis, S. N. and Robinson, A. L.: A two-dimensional volatility basis set: 1. organic-aerosol mixing thermodynamics, Atmos. Chem. Phys., 11(7), 3303–3318, doi:10.5194/acp-11-3303-2011, 2011.

Greco, G., Grosse, S. and Letzel, T.: Serial coupling of reversed-phase and zwitterionic hydrophilic interaction LC / MS for the analysis of polar and nonpolar phenols in wine, J. Sep. Sci., 36, 1379–1388, doi:10.1002/jssc.201200920, 2013.

Harper, M.: Sorbent trapping of volatile organic compounds from air, J. Chromatogr. A, 885(1–2), 129–151, doi:10.1016/S0021-9673(00)00363-0, 2000.

Jimenez, J. L., Canagaratna, M. R., Donahue, N. M., Prevot, A. S. H., Zhang, Q., Kroll, J. H., Decarlo, P. F., Allan, J. D., Coe, H., Ng, N. L., Aiken, A. C., Docherty, K. S., Ulbrich, I. M., Grieshop, A. P., Robinson, A. L., Duplissy, J., Smith, J. D., Wilson, K. R., Lanz, V. A., Hueglin, C., Sun, Y. L., Tian, J., Laaksonen, A., Raatikainen, T., Rautiainen, J., Vaattovaara, P., Ehn, M., Kulmala, M., Tomlinson, J. M., Collins, D. R., Cubison, M. J., Dunlea, E. J., Huffman, J. A., Onasch, T. B., Alfarra, M. R., Williams, P. I., Bower, K., Kondo, Y., Schneider, J., Drewnick, F., Borrmann, S., Weimer, S., Demerjian, K., Salcedo, D., Cottrell, L., Griffin, R., Takami, A., Miyoshi, T., Hatakeyama, S., Shimono, A., Sun, J. Y., Zhang, Y. M., Dzepina, K., Kimmel, J. R., Sueper, D., Jayne, J. T., Herndon, S. C., Trimborn, A. M., Williams, L. R., Wood, E. C., Middlebrook, A. M., Kolb, C. E., Baltensperger, U. and Worsnop, D. R.: Evolution of Organic Aerosols in the Atmosphere, Science., 326, 1525–1529, 2009.

Kenagy, H. S., Sparks, T. L., Ebben, C. J., Wooldrige, P. J., Lopez-Hilfiker, F. D., Lee, B. H., Thornton, J. A., McDuffie, E. E., Fibiger, D. L., Brown, S. S., Montzka, D. D., Weinheimer, A. J., Schroder, J. C., Campuzano-Jost, P., Day, D. A., Jimenez, J. L., Dibb, J. E., Campos, T., Shah, V., Jaeglé, L. and Cohen, R. C.: NOx Lifetime and NOy Partitioning During WINTER, J. Geophys. Res. Atmos., 123(17), 9813–9827, doi:10.1029/2018JD028736, 2018.

Khare, P., Marcotte, A., Sheu, R., Walsh, A. N., Ditto, J. C. and Gentner, D. R.: Advances in offline approaches for trace measurements of complex organic compound mixtures via soft ionization and high-resolution tandem mass spectrometry, J. Chromatogr. A, 1598, 163–174, doi:10.1016/j.chroma.2019.03.037, 2019.

Pagonis, D., Krechmer, J. E., de Gouw, J., Jimenez, J. L. and Ziemann, P. J.: Effects of gas–wall partitioning in Teflon tubing and instrumentation on time-resolved measurements of gas-phase organic compounds, Atmos. Meas. Tech., 10(12), 4687–4696, doi:10.5194/amt-10-4687-2017, 2017.

Petters, M. D. and Kreidenweis, S. M.: A single parameter representation of hygroscopic growth and cloud condensation nucleus activity, Atmos. Chem. Phys., 8, 1961–1971, doi:10.5194/acpd-6-8435-2006, 2007.

Pyke, J. S., Callahan, D. L., Kanojia, K., Bowne, J., Sahani, S., Tull, D., Bacic, A., McMonville, M. J. and Roessner, U.: A tandem liquid chromatography – mass spectrometry (LC – MS) method for profiling small molecules in complex samples, Metabolomics, 11(6), 1552–1562, doi:10.1007/s11306-015-0806-7, 2015.

Ramírez, N., Cuadras, A., Rovira, E., Borrull, F. and Marce, R. M.: Comparative study of solvent extraction and thermal desorption methods for determining a wide range of volatile organic compounds in ambient air, Talanta, 82, 719–727, doi:10.1016/j.talanta.2010.05.038, 2010.

Ras, M. R., Borrull, F. and Marce, R. M.: Sampling and preconcentration techniques for determination of volatile organic compounds in air samples, , 28(3), 347–361, doi:10.1016/j.trac.2008.10.009, 2009.

Rogers, H. M., Ditto, J. C. and Gentner, D. R.: Evidence for impacts on surface-level air quality in the northeastern US from long-distance transport of smoke from North American fires during the Long Island Sound Tropospheric Ozone Study (LISTOS) 2018, Atmos. Chem. Phys., 20(2), 671–682, doi:10.5194/acp-20-671-2020, 2020.

Sheu, R., Marcotte, A., Khare, P., Charan, S., Ditto, J. C. and Gentner, D. R.: Advances in offline approaches for chemically speciated measurements of trace gas-phase organic compounds via adsorbent tubes in an integrated sampling-to-analysis system, J. Chromatogr. A, 1575, 80–90, doi:10.1016/j.chroma.2018.09.014, 2018.

Slade, J. H., Ault, A. P., Bui, A. T., Ditto, J. C., Lei, Z., Bondy, A. L., Olson, N. E., Cook, R. D., Desrochers, S. J., Harvey, R. M., Erickson, M. H., Wallace, H. W., Alvarez, S. L., Flynn, J. H., Boor, B. E., Petrucci, G. A., Gentner, D. R., Griffin, R. J. and Shepson, P. B.: Bouncier Particles at Night: Biogenic Secondary Organic Aerosol Chemistry and Sulfate Drive Diel Variations in the Aerosol Phase in a Mixed Forest, Environ. Sci. Technol., 53(9), 4977–4987, doi:10.1021/acs.est.8b07319, 2019.

Zhou, S., Collier, S., Xu, J., Mei, F., Wang, J., Lee, Y.-N., Sedlacek, A. J., Springston, S. R., Sun, Y. and Zhang, Q.: Influences of upwind emission sources and atmospheric processing on aerosol chemistry and properties at a rural location in the Northeastern U.S., J. Geophys. Res. Atmos., 121(10), 6049–6065, doi:10.1002/2015JD024568, 2016.